

High-Speed LIF-OH Imaging in Premixed Flames Propagating Past Repeated Solid Obstacles

A. AlHarbi^{*}1, M. Juddoo¹, and A.R. Masri¹

¹School of Aerospace, Mechanical and Mechatronic Engineering,
The University of Sydney, NSW 2006, Australia

Abstract

This paper presents high-speed imaging of laser induced fluorescence from OH (HS-LIF-OH), with a repetition rate of 5 kHz performed in a chamber where premixed flames are propagating past a range of solid obstacles. The chamber geometry is identical to that used in earlier studies but the fuels studied here are compressed natural gas (CNG) at unity equivalence ratio, $\phi=1$ and hydrogen with $\phi=0.7$. The leading edge of the OH is taken as a marker of the reaction zone which is tracked in time to determine the flame's spatial structure and rate of propagation. It is confirmed that the burning rate for CNG is much slower than hydrogen as is consistent with the differences in laminar flames speed for these two fuels. It is noted that transition to a turbulent flame structure with intense corrugations does not occur in the presence of just one obstacle. Additionally, the separation between successive baffles is important to induce faster burning rates since the re-laminarisation effects is quite fast. In general, it is found that for the same sequence of obstacles, hydrogen flames result in less wrinkled flame fronts than CNG as is evident from the resulting images. This may be potentially due to the lower Reynolds numbers with hydrogen flames resulting from the lower densities.

1. Introduction

The work presented here is a continuation of a long-standing effort to enhance current understanding of premixed flame propagation and their interactions with repeated solid obstacles [1-3, 14-16, 18]. The long term objective is to develop reliable computational capabilities to calculate the structure of such flows and predict the overpressures resulting for these deflagrations interacting with blockages and surfaces. This is an issue of practical relevance not only to the design of premixed combustors but also in industrial safety where minimising and containing the risk of explosions is of prime importance.

Modelling of turbulent propagating premixed flames has advanced significantly over the past decades [4, 8, 10, 20], thanks largely to the bank of experimental data that has recently become available. Moen et al. [18] used large scale experiments to study the effects of obstacles sizes on the propagation of premixed flame of Methane and concluded that the flame speed could increase by up to 24 times the velocity obtained with no obstacle. Laboratory studies have explored a range of geometries in enclosed cylindrical vessels with or without obstacles [22, 23], cylindrical vessels with turbulence inducing rings [2, 3] or circular plate obstructions [21] chambers with a rectangular cross-section using a single plate as an internal baffle [13] or with a square cross-section and multiple baffles lining the top and bottom walls of the chamber [11]. Alexiou et al. [1] studied the effects of positioning the vent on the side or at the end of a cylindrical vessel. Patel et al. [20] studied deflagrations in a

square cross-section chamber using flat plates as obstacles placed repeatedly at various distances along the chamber's length.

Masri and co-workers have reported extensively on the effects of repeated solid obstacles on the structure and rate of propagation of turbulent premixed flames [14-16, 5, 6, 12]. The experimental chamber used has a square cross section with an overall volume of 0.625 litres and a length to width ratio of $L/W = 5$. Earlier configurations [12] have used a larger chamber with a volume of 20 litres and L/W ratio of 2.8. The fuel used in these studies is largely LPG and to a lesser extent, compressed natural gas (CNG). High-speed planar images of laser induced fluorescence from OH (HS-LIF-OH) has revealed interesting features about the structure of the flame as it propagates along the chamber and past the repeated obstacles [16, 17].

Recent interest in hydrogen as a clean fuel for powering fuel cell vehicles (FCV) [7, 19] has raised serious concerns about hydrogen safety. This is particularly relevant considering that hydrogen is highly reactive with broader flammability limits than most hydrocarbon fuels. The potential of hydrogen leaks and subsequent explosions in tunnels, refueling stations, etc...necessitates a better understanding of the behavior of premixed propagating flames of hydrogen. In a recent paper [16], peak overpressures and rates of pressure rise were reported for LPG, CNG and lean hydrogen flames using the same experimental chamber studied here. It was found that, for the same configuration of obstacles, the rate of pressure rise for even lean hydrogen flames is orders of magnitudes higher than that measured for stoichiometric flames of CNG and LPG.

The present contribution uses the same experimental chamber to report the first high-speed planar images of laser induced fluorescence from OH (HS-LIF-OH) obtained in turbulent propagating flames of hydrogen. LIF-OH is used here for convenience as a marker of the reaction front and the images are collected at a repetition rate of 5 kHz. Four cases are studied here with increasing number of obstacles and the structure of the reaction zone is discussed.

2. Experimental

2.1 The Combustion Chamber and Configurations

The same combustion chamber used in earlier studies is adopted here for convenience. It is square in cross-section with internal dimensions of length, $L = 250$ mm and side, $W = 50$ mm producing an overall volume of 0.625 Litres and a ratio $L/W = 5$. Full details of the combustion chamber are published earlier [20]. Two different fuels are used here: hydrogen and compressed natural gas (CNG with 88.8% CH_4 , 7.8% C_2H_6 , 1.9% CO_2 and 1.2% N_2 with the remaining 0.3% being a mixture of propane, propane, butane and pentane). The fuel-air mixture enters the atmospheric pressure chamber through a non-return valve. The

operating conditions in preparation for each combustion event are optimised to ensure repeatability and the process is described here as follows: Before each ignition event, the fuel air mixture is injected for 10 seconds at a flow rate of 27.8 l/min. The flow is then stopped and the gases within the chamber are allowed to settle for 15 second (CNG) and 5 seconds (H₂) before the stagnant mixture is ignited by focusing the infrared output from a Nd:YAG laser 2 mm above the chamber's base. Laser timing is controlled by the Q-switch of the Nd:YAG and this marks the start of each experiment, or time zero.

For CNG, a stoichiometric equivalence ratio is used throughout, $\phi=1$ while for hydrogen, lean mixtures with $\phi=0.7$ are adopted since stoichiometric mixtures result in excessively high pressures. A wide range of configurations are studied but only four are reported here and these are shown in Fig. 1. Three baffle plates may be used each consisting of five strips, 4 mm wide, evenly separated by six gaps, 5 mm wide, thus creating an overall blockage ratio of 0.4. Downstream of the baffle plates, a further obstruction with a square cross section of 12×12 mm may be placed such that its lower surface is maintained at 91mm from the base plate. Configuration 000S uses only the small solid obstacle without any baffle plates while configurations b00S, bb0S and bbbS have, respectively one, two and three baffle plates in addition to the small obstacle.

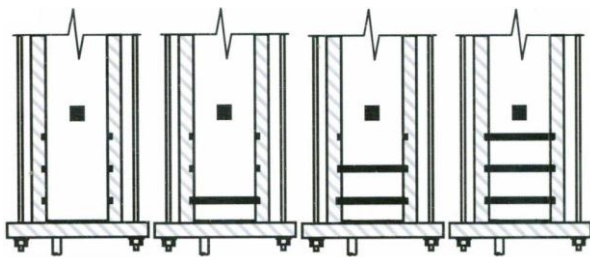


Figure 1: Schematics of configurations 000S, b00S, bb0S and bbbS.

2.2 High-Speed LIF-OH Imaging

A schematic of the high speed LIF-OH imaging set-up which excites the $Q_1(6)$ line of the $A^2\Sigma \leftarrow X^2\Pi(1,0)$ system at 283.01 nm is shown in Figure 2a. An Edgewave (IS411-E) Nd:YAG laser, with a power of 12W and a pulse length of around 10ns is used to pump a SIRAH Allegro high-speed dye laser. The dye used was Rhodamine 6G in ethanol, and produced a fundamental beam at 566 nm, which was then frequency doubled using a BBO crystal to produce a UV beam at 283nm. The first and second harmonics were separated using a set of 4 Pellin-Broca prisms with a resulting output average power of 750 mW at 5 kHz (150 μ J/pulse). The beam was then expanded to 75 mm in height using a diverging cylindrical lens before being focused into a sheet at the imaging axis using a fused-silica focusing lens with a 300 mm focal length.

The detection system consists of a LaVision High-Speed-Star 6 (HSS6) CMOS camera with a lens-coupled two-stage intensifier (High-Speed IRO: Intensified Relay Optics, LaVision) that has its highest sensitivity in the UV range. The camera was run at a repetition rate of 5 kHz with an array of 1024 x 1024 pixels and the intensifier had a gate width of 200 ns. The CMOS on-board memory of 8GB can hold just over 5000 frames at 5 kHz, corresponding to an acquisition time of 1s. The repetition rate was high enough to capture flame front propagation from shot-to-shot. The OH-PLIF signals were collected using two sets of LAPQ/APMQ (CVI product) three-element UV lenses, with a clear aperture of 60mm. The lenses were coupled back-to-back, and placed in front of the HSS6 camera, along with WG 305 and WG295 interference filters. The imaged area was 50 mm x 75

mm, thus covering the whole height of the laser sheet but not the entire chamber. To do so, it was necessary to select two imaging windows which overlap slightly as shown in Figure 2b. For each case, the imaging process was repeated two times to cover each of imaging windows T1 and T2.

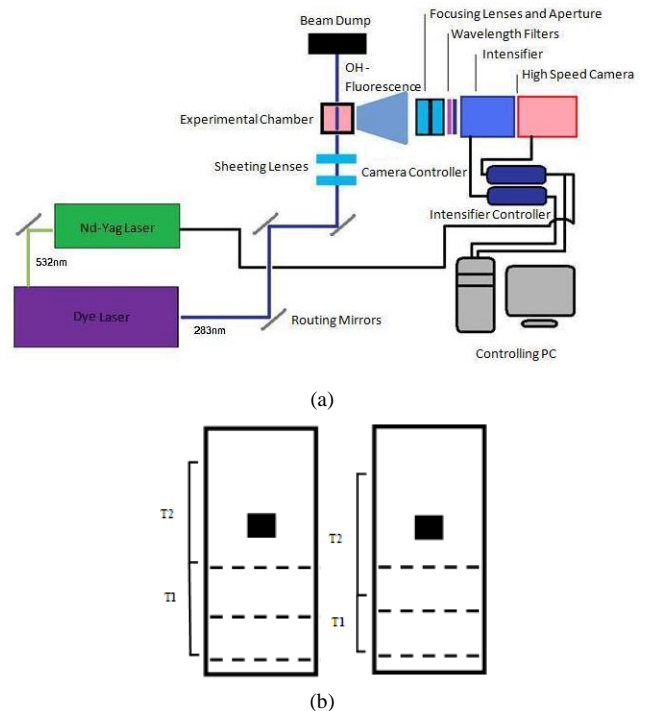


Figure 2: (a) Schematic of the high speed LIF-OH imaging equipment (b) the two imaging tiers used to capture the maximum viewable height. [RHS used for configuration bbbS, LHS for the rest of configurations]

3. High-Speed LIF-OH Images

Thousands of images are collected for each configuration and these may be made available on request. Only a very small representative sample may be shown here to highlight the general features of the flame. Figures 3 and 4 show an image sequence of LIF-OH measured in each of the four configurations studied here. The sequence is collected in window T2 which covers the region starting from around the third baffle plate to well downstream the square obstacle (see Fig. 2b). Note that the images are blanked on the right hand side of the square obstacle because the laser sheet is blocked in that region. The image sequences shown here are separated by a minimum of 0.2ms (as dictated by the repetition rate of 5 kHz) although in some configurations (such as b00s and 000s CNG) a larger separation of 0.6ms is shown because little variation was noted between successive frames.

Results for CNG are presented in Fig. 3 while those for hydrogen are shown in Fig. 4. The flame front reaches the imaging window T2 at different time depending on the fuel and the configuration and this is noted for each image in Figs. 3 and 4. For CNG, imaging in window T2 commenced some 15.6ms and 11ms after ignition for configurations 000S and bbbS, respectively. For hydrogen, however, the times are much shorter due to the higher flame speeds and these range from 5.2ms for configuration 000S to 4.0ms for bbbS. It is worth noting also that between configurations 000S and bbbS, the increase in flame speed is higher for hydrogen than for methane as is reflected in the times taken for the flame front to cross the imaging window, T2. These times for hydrogen range from 1.2ms for case 000S and 0.2ms for bbbS. The comparison times for CNG are 3ms for configuration 000S and about 1ms for bbbS.

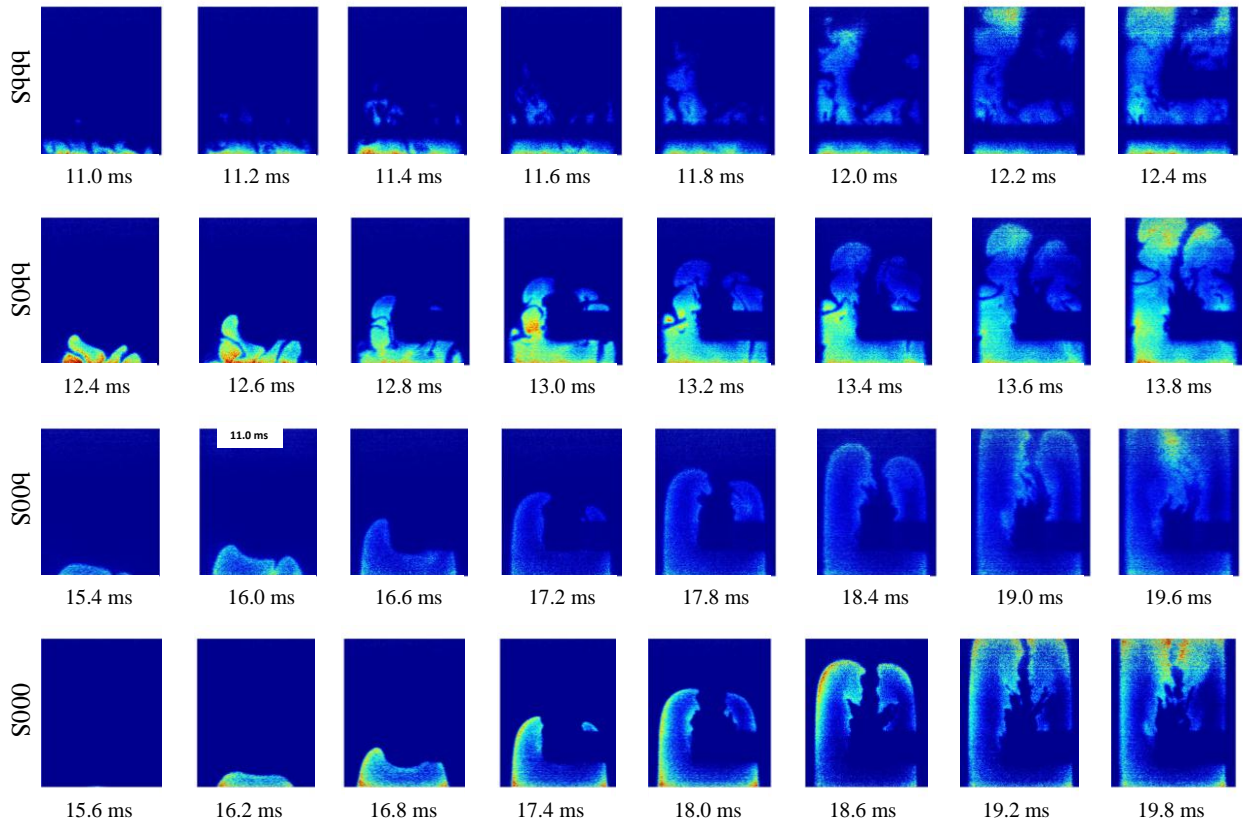


Figure 3: Time sequences for different CNG configurations in 0.2 ms steps (bbbS, bb0S) and 0.6 ms steps (b00S, 000S)

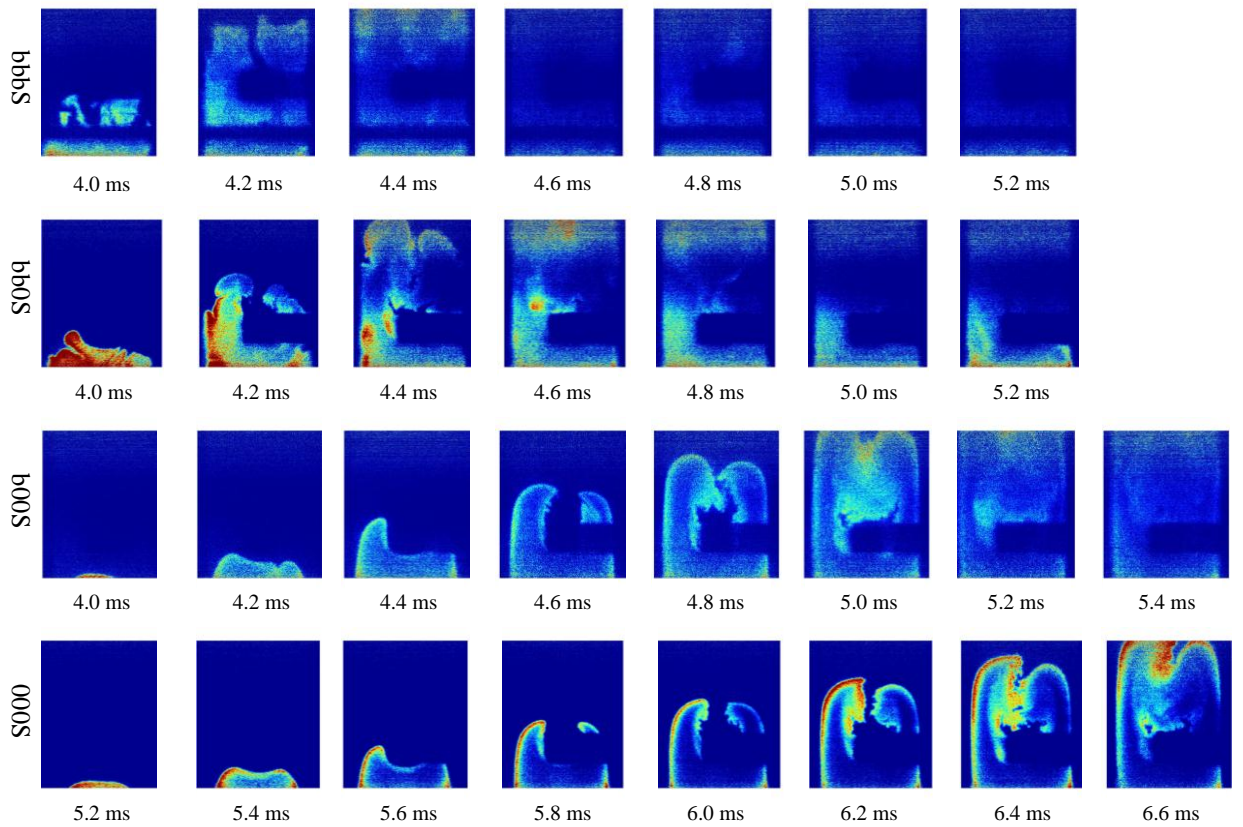


Figure 4: Time sequences for different Hydrogen configurations in 0.2 ms steps (bbbS, bb0S, b00S and 000S)

Images for configurations 000S and b00S show similar features for both hydrogen and CNG fuels in that the flame front looks somewhat laminar as it exits the channel and then wrinkles and corrugates slightly as it recirculates downstream the square obstacle. It should also be noted that for case b00S, whatever turbulence was introduced through the first baffle was dissipated due to the higher viscosity so the flame front re-laminarises before reaching the square obstacle.

Cases bb0s and bbbS show a different flame structure since the second (and third) baffle increase the turbulence before the flame reaches the obstacle. Both CNG and hydrogen flames show an increase in the level of flame corrugation as is evident from the images shown for 12.4 to 13.0ms (case bb0S, CNG) and 4 to 4.4ms (case bb0S, hydrogen). Adding the third baffle (case bbbS) increases turbulence even further and the flame speeds up and becomes more contorted and even fragmented as shown for case bbbS (CNG) at 11.4 to 12.0ms. Note here that for the same case (bbbS) but with hydrogen fuel, the flame travels very quickly so the 5kHz system is not sufficiently fast to see full details of its evolution.

While based only on the qualitative appearance of the images, it appears that for the same configuration, (say bb0S or bbbS), hydrogen flames are less wrinkled than the CNG counterparts. Based on a length scale of 2.5mm (half the width of the opening in the baffle plates) the Reynolds numbers of the non-reacting mixtures corresponding to CNG and hydrogen are 151.8*V and 23.0*V respectively. So, for the same velocity V=50 m/s, the Reynolds numbers for CNG and hydrogen are 7590 and 1150 and this may partly explain the higher level of wrinkling in CNG. This is highly speculative and further research is needed to confirm this. While the details presented in these LIF-OH images are new and confirm earlier results [13, 16] regarding the increased level of wrinkling with increasing blockage, higher camera speeds are needed to better resolve the flame fronts in the hydrogen flames

4. Conclusions

Propagation of turbulent premixed flames past solid obstacles are investigated for CNG and hydrogen fuel mixtures. High-speed LIF-OH imaging applied for a range of configurations with different obstacles reveal an increase in the level of flame wrinkling with increasing blockage. Hydrogen flames are much faster than CNG although, for the same configuration of obstacles, the corrugation in the flame front appears to be less significant for hydrogen flames. It is also evident from the LIF-OH images that the flame front re-laminarises as the separation between successive obstacles increases.

Acknowledgments

This work is supported by the Australian Research Council. The assistance of Dr. Sten Starner is highly appreciated.

References

- [1] Alexiou, A., Andrews, G.E. and Phylaktou, H., Side-vented gas explosions in a long vessel: the effect of vent position. *Journal of Loss Prevention in the Process Industries*. **1996**, *9*, 351-356.
- [2] Fairweather, M., Hargrave, G.K., Ibrahim, S.S. & Walker, D.G., Studies of premixed flame propagation in explosion tubes. *Combust. Flame*. **1999**, *116*, 504-518.
- [3] Fairweather, M., Ibrahim, S.S., Jagers, H. & Walker, D.G., Turbulent premixed flame propagation in a cylindrical vessel. *Proc. Combust. Inst.* **1996**, *26*, 365-371.
- [4] Gubba, S.R., Ibrahim, S.S., Malalasekera, W. & Masri, A.R., An assessment of large eddy simulations of premixed flames propagating past repeated obstacles, *Combust. Theory Modell.* **3**, 2009, 513-540
- [5] Hall, R., Influence of obstacle location and frequency on the propagation of premixed flames, Postgraduate Thesis, *School of Aerospace, Mechanical and Mechatronic Engineering*, University of Sydney, 2008
- [6] Hall, R., Masri, A.R., Yaroshchyk, P. & Ibrahim, S.S., Effects of position and frequency of obstacles on turbulent premixed propagation flame, *Combustion and Flame*, **156**, 2009, 439 - 446
- [7] Hirose, K., Hydrogen as a fuel for today and tomorrow: expectations for advanced hydrogen storage materials/system research, *Journal of Faraday Discussions*, **151**, 2011, 11-18
- [8] Ibrahim, S.S. & A. R. Masri, The effects of obstructions on overpressure resulting from premixed flame deflagration, *Journal of Loss Prevention in the Process Industries*, **14**, 2001, 213 - 221
- [9] Ibrahim, S.S., Gubba, S.R., Masri, A.R., & Malalasekera, W., Calculation of explosion deflection flame using a dynamic flame surface density model, *Journal of Loss Prevention in the Process Industries*
- [10] Ibrahim, S.S., Hargrove, G.K. and Williams, T.S., Experimental investigation of flame/solid interaction in turbulent premixed combustion, *Experimental Thermal and Fluid Science*, **24**, 2001, 99 - 106
- [11] Johansen, C.T. & Ciccarelli, G., Visualization of the unburned gas flow field ahead of an accelerating flame in an obstructed square channel. *Combust. Flame*. **2009**, *156*, 405-416.
- [12] Kent, J.E., Masri, A.R., & Starner, S.H., A New Chamber to Study Premixed Flame Propagation Past Repeated Obstacles, in *5th Asia-Pacific Conference on Combustion* The University of Adelaide, Adelaide, Australia, 2005.
- [13] Lindstedt, R.P. & Sakthitharan, V., Time Resolved Velocity and Turbulence Measurements in Turbulent Gaseous Explosions. *Combust. Flame*. **1998**, *114*, 469-483.
- [14] Masri, A.R., Ibrahim, S.S. & Cadwallader, B.J., Measurements and large eddy simulation of propagating premixed flames, *Experimental Thermal and Fluid Science*, **30**, 2006, 687 - 702
- [15] Masri, A.R., Ibrahim, S.S., Nehzat, N. & Green, A.R., Experimental study of premixed flame propagation over various solid obstructions, *Experimental Thermal and Fluid Science*, **21**, 2000, 109-116
- [16] Masri, A.R., AlHarbi, A.A., Meares, S. & Ibrahim, S.S., A comparative Study of Turbulent Premixed Flames Propagation Past Repeated Obstacles, *Journal of Industrial and Engineering Chemistry Research*, **51**, 2012, 7690-7703
- [17] Meares, S., AlHarbi, A.A. & Masri, A.R., High-Speed LIF-OH Imaging of Turbulent Premixed Flames Propagation Past Solid Obstacles, 8th Asia-Pacific Conference on Combustion, 2010, 814-821
- [18] Moen, I.O., Donato, M., Knystautas, R. & Lee, J.H., Flame acceleration due to turbulence produced by obstacles, *Combust. Flame*, **39**, 1980, 21-32
- [19] Ogdens, J., Steinbugle, M. & Kreutz, T., A comparison of hydrogen and gasoline as fuels for fuel cell vehicles: implications for vehicle design and infrastructure development, *Journal of Power Sources*, **79**, 1999, 143-168
- [20] Patel, S.N.D.H., Jarvis, S., Ibrahim, S.S. & Hargrave, G.K., An experimental and numerical investigation of premixed flame deflagration in a semiconfined explosion chamber. *Proc. Combust. Inst.* **2002**, *29*, 1849-1854.
- [21] Phylaktou, H. & Andrews, G.E., The acceleration of flame propagation in a tube by an obstacle. *Combust. Flame*. **1991**, *85*, 363-379.
- [22] Starke, R. & Roth, P., An experimental investigation of flame behavior during explosions in cylindrical enclosures with obstacles. *Combust. Flame*. **1989**, *75*, 111-121.
- [23] Starke, R. & Roth, P., An experimental investigation of flame behavior during cylindrical vessel explosions. *Combust. Flame*. **1986**, *66*, 249-259